

**A first principles study on the ferroelectric properties of the
phases of hafnia.**

B.F. Horsman

Supervised by:

Prof. Dr. G. Koster

Dr. A. van Houselt

C.A.J. de Hond MSc

Inorganic Materials Science
University of Twente
The Kingdom of the Netherlands
20-08-2021

Contents

1	Introduction	2
1.1	Introduction to ferroelectricity	2
1.2	Research questions of the thesis	4
2	Theory and literature	5
2.1	Literature on hafnia	5
2.2	Phonons and phonon plots	8
2.3	Density Functional Theory	10
3	Methods and setup	14
3.1	Introduction to VASP	14
3.2	Retrieving energy values	18
3.3	Computing phonon dispersion relations	18
3.4	Epitaxially strained hafnia	19
4	Results	21
4.1	Reproduction of past research	21
4.1.1	Energy values of the hafnia phases	21
4.1.2	Phonon dispersion relations of the hafnia phases	22
4.2	Energy values and phonon spectra of the R3m phase of hafnia on GaN	27
4.3	Properties of R3m phase hafnia grown on GaN	29
5	Conclusion	34
6	Discussion	35
	Bibliography	36
A	The jobscript of the ionic relaxation of the R3m phase of hafnia constrained on SrTiO₃ and GaN	39

1 Introduction

1.1 Introduction to ferroelectricity

In condensed matter physics many different theories and phenomena have been discovered throughout time. One of those phenomena is ferroelectricity. The phenomenon of ferroelectricity was discovered just over a hundred years ago in 1920 by Joseph Valalesk, a PhD student at the University of Minnesota, Minnesota, USA [1] [2]. Valalesk studied Rochelle salt, potassium sodium tartrate tetrahydrate, and its piezoelectric properties in order to try to develop a seismograph. Piezoelectric materials generate electric charge when put under mechanical stress and vice versa. However, when Valalesk set the electric polarization out as a function of the electric field it showed hysteresis, which is shown in figure 1. The salt was always electrically polarized and the direction of the electric polarization could be inverted by applying an electric field opposite to the polarization. This is the basis of ferroelectricity. Since the experimental discovery of ferroelectricity a theory behind it has been developed and many new materials have been found to possess ferroelectric properties. Also many daily life appliances make use of ferroelectric materials. The concept of ferroelectricity is nowadays used in magnetic-field detectors, piezoelectric nanotubes, high-energy capacitors, night-vision technology, medical ultrasound devices and energy harvesting [3].

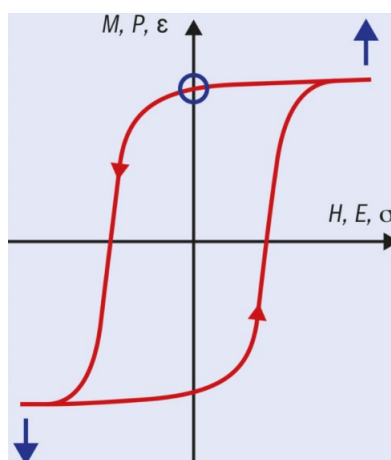


Figure 1: The hysteresis loop seen in ferroelectric materials. This kind of hysteresis loop can also be seen in ferromagnetics and ferroelastics, indicated by respectively M vs. H and ϵ vs. σ . Adapted from [2].

The concept behind ferroelectricity can be explained using one of the now used material groups used in ferroelectric appliances: perovskites. Zooming in on the perovskite lead zirconate titanate ($\text{PbZr}_x\text{Ti}_{1-x}\text{O}_3$), in general named PZT, the unit cell of the standard stable cubic phase is drawn in figure 2a. In its stable phase, PZT is not ferroelectric. This is to be expected since the symmetry in the unit cell is such that there is no net dipole moment. However, if the temperature of a fragment of PZT is lowered to a point where the temperature is lower than the Curie Temperature, it undergoes a phase transformation. It then transforms into a tetragonal structure, as can be seen in figure 2b. That in itself is not a cause for the ferroelectric behaviour of PZT. During the phase

transition, in addition to the structure transformation, the structure becomes asymmetric, as the Titanium or Zirconium ion in the center of the unitcell becomes displaced. Now that the symmetry is broken, the unit cell has a nonzero dipole moment and so an electric polarization and an electric dipole. The cause of the ferroelectricity is hence the fact that symmetry is broken. In a piece of material of PZT it over all might not directly have a dipole moment due to the misalignment of the individual dipoles. With a strong electric field however one can align the individual dipoles and so an effective dipole moment is caused.

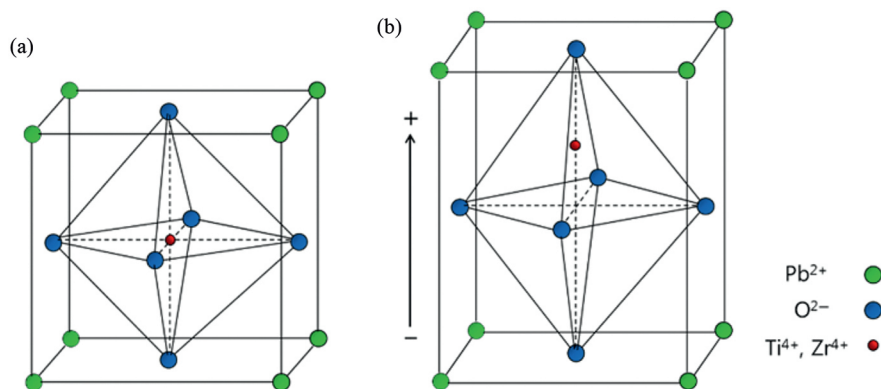


Figure 2: 2a. The standard stable cubic phase of PZT 2b. The asymmetric tetragonal phase below the Curie temperature. Adapted from [4].

Since the experimental discovery of ferroelectricity a theory behind it has been developed and many new materials have been found to possess ferroelectric properties. This process is still going on, as some materials are more fit for applications than others. PZT for example is a very effective ferroelectric material. However, for some applications where the length scale for where ferroelectric properties are the most prominent materials with a high(er) dielectric constant are sometimes preferred over PZT [5]. Furthermore PZT does contain lead, which is not environment friendly and lead is considered a (moderately) scarce metal [6] [7], so it may be more expensive to mine and harder to get. Here hafnia (HfO₂) comes in to play. Hafnia is a material that does show ferroelectricity, which was discovered at the beginning of the last decade. Hafnia is more environment friendly due to not containing lead and hafnia shows potential to have a polarization that for some appliances that is preferable over PZT given certain conditions [5][3]. In thin films this could be used to shrink the size of specific layers up down to 10 nm or even smaller [5]. Since the literature of ferroelectricity of hafnia only goes back to the early 2010s, it is still a topic under research. In 2018 researchers from the University of Groningen discovered new ferroelectric phases [8]. In this bachelor thesis I try to set up a method of calculations such that the energy of the various phases of hafnia, their dipole moment, and the corresponding phonon bands can be calculated. This to verify research done in the past and to be able to make a computational estimates of thin films arrangements which will be researched experimentally.

1.2 Research questions of the thesis

As this kind of computational research is new within the Inorganic Materials Science (IMS) research group I will, together with my supervisors, try to set up a robust way to do phonon-band, energy and polarization calculations on thin films under epitaxial strain. Our material subject will be pure hafnia as it is a current research topic. The calculations will be done with pure hafnia, as doped hafnia, which usually is done, complicates the computational simulations greatly due to complexity and the computational load. The computations will be done using (001)-oriented hafnia to further simplify the computations. Using the upper methods we will try to determine a relation between the polarization values when the rhombohedral R3m phase of hafnia is grown on SrTiO₃ and GaN, as it and interest lies in the rhombohedral R3m (and R3) phase as it was only discovered three years ago by the University of Groningen and is in research now too at the University of Twente. This results in the following research questions with the last one being the main research question:

- Can we reproduce phonon spectra and energy values of the various hafnia phases from the past research?
- Can we compute phonon spectra and find the energy value of the R3m hafnia phase when put under epitaxial strain attributed to SrTiO₃ ?
- By applying epitaxial strain, corresponding to a substrate of SrTiO₃ and GaN, on the pure R3m phase of hafnia can we find an relation between the c-lattice vector and the energy, the specific substrate and its polarization values?

2 Theory and literature

The theory in this section gives some background on hafnia and some principles used to find answers to the research questions.

2.1 Literature on hafnia

The research on the topic of ferroelectricity of hafnia has developed rapidly since the early 2010s. The fact that, with respect to the research done on PZT, it took such a long time before ferroelectricity in hafnia was discovered stems from the fact that the origin of ferroelectricity in hafnia is more complex, more complex than presented for PZT in figure 2. The precise mechanism where ferroelectricity originates from in hafnia is still not fully known. Hafnia is a polymorphic material and hence can adopt various crystalline phases. The stable phase at atmospheric pressure and room temperature is a monoclinic phase ($P2_1/c$) [5]. Other phases of hafnia include: cubic phases ($Pa\bar{3}$ and $Fm\bar{3}m$) a tetragonal phase ($P4_2/nmc$) and multiple orthorhombic phases (of which $Pmn2_1$ and $Pca2_1$ are of interest). A phase diagram of the various phases of hafnia and the unit cell of hafnia in the stable monoclinic phase can be seen in respectively figure 3 and 4. Besides the phases given, Wei et al. [8] found two more phases of interest which cannot be seen in the phase diagram. Specifically two rhombohedral phases ($R3$ and $R3m$). This is due to their relatively high energy with respect to the other phases.

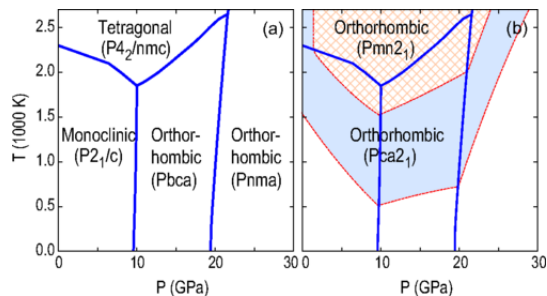


Figure 3: The left figure shows a standard phase diagram of hafnia. The right figure shows the phases of hafnia with slightly higher free energy (of the order $k_B T/5$). Adapted from [9].

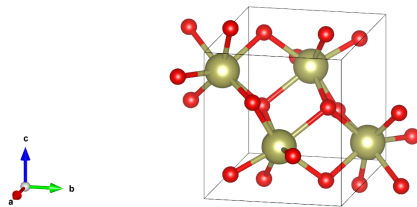


Figure 4: Primitive unit cell of the $P2_1/c$ monoclinic phase of hafnia. Generated using computed data by [10].

As non-centrosymmetry is required for material phases to show properties of ferroelectricity, only the orthorhombic and rhombohedral phases are of interest. Indeed all of these phases show ferroelectric properties. The ferroelectric properties of the orthorhombic phases of hafnia were discovered around 2014. The two orthorhombic phases are not stable, but their energy level is close to the energy level of the stable phases. It differs only by an order of $\frac{k_B T}{5}$, as can be seen in figure 3, where T is taken at room temperature. The unit cell of the $Pca2_1$ can be seen in figure 5. The ferroelectric properties of hafnia are different from usual ferroelectrics. In general the ferroelectric properties of thin films diminish if the thickness decreases, but for both the orthorhombic (and rhombohedral) phases of hafnia this is not the case. Orthorhombic phases of hafnia are present in thin films of (approximately) 10 nm . For thicker thin films the non-ferroelectric monoclinic phase appears and coexists with the orthorhombic phase. This lowers the possible polarization of the thin film. The properties of the 10 nm orthorhombic phase thin films also show up for larger thin films in the range of $50 - 300\text{ nm}$ where the average grain size is (approximately) 10 nm . Computational simulations using the two phases suggest that the electric polarization of the two orthorhombic phases might reach respectively $P_{Pca2_1} = 52\ \mu\text{C}/\text{cm}^2$ and $P_{Pmn2_1} = 56\ \mu\text{C}/\text{cm}^2$. The ferroelectric properties of the orthorhombic $Pca2_1$ phase can be observed in figure 6. The relation between the energy and the polarization is of the form of a double-well potential. It is of the form $E = aP^2 + bP^4$ where a and b are constants. This is conform the Landau-Ginzburg second order phase transition formalism [11]. The $Pca2_1$ phase is stable in both minimums at $P_{Pca2_1} = 52\ \text{C}/\text{m}^2$. Note that the two stable situations for the $Pca2_1$ phase are $104\ \text{C}/\text{m}^2$ apart as the reference point for the (maximum) polarization is the maximum in figure 6 at $P = 0\ \text{C}/\text{m}^2$ [5]. The barrier between the two stable situations can be overcome by applying an electric field opposite to the polarisation over the the material. This is called the polarisation reversal process. The electric field increases the potential energy of the phase and decreases the (absolute) polarisation. At the same time within the unit cell of the Pca_1 phase the atom positions and geometry change, which also can be observed in figure 6. During the transformation process the O atoms in the unit cell move along the c -axis relative to the Hf atom. The maximum in the energy versus polarization corresponds to the situation where the structure of the unit cell being centrosymmetric as the Hf atom now lies within the plane of the moving O atoms. This actually is a phase change to the tetragonal $P4_2/nmc$ phase. This is the parent phase of both of the ferroelectric orthorhombic phases of hafnia. The trajectory of the moving O atoms is parabolic. The origin of that lies in the strong bonds between the O and Hf atoms, which forms a trapezoid atomic pattern when in a stable regime. During the polarisation reversal process the orientation of the unit cell changes and becomes the opposite of what it was. A left orientation of the trapezoid will become a right orientation and vice versa.

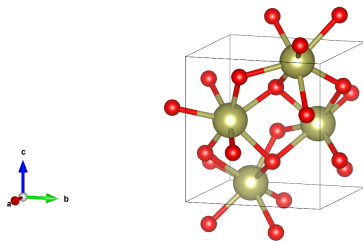


Figure 5: Primitive unit cell of the $Pca2_1$ orthorhombic phase of hafnia. Generated using computed data by [10].

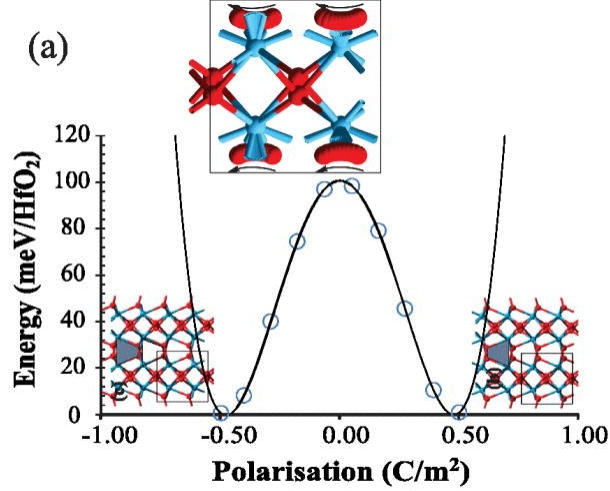


Figure 6: The relation between the energy and the polarisation for the $Pca2_1$ orthorhombic phase of hafnia together with an example of the deformation process. The circles in the plot represent data points of simulations. Adapted from [5].

As mentioned before there are also two rhombohedral phases that show ferroelectric properties (computationally), the R3 and the R3m phase. The ferroelectric properties of a rhombohedral phase of hafnia were discovered in 2018 by Wei et al. [8]. Wei et al. suggest that, by DFT-calculations, the phase found was either a doping-poor R3 phase or an R3m phase under epitaxial compression. The thin films were found to be predominantly (111)-oriented. A unit cell of the R3m phase is shown in figure 7. These phases were left untreated by Doan Huan et al. [9]. One does not see them back in figure 3. This can be explained by the larger energy difference between the stable monoclinic phase and the R3m / R3 phase with respect to the energy difference between the monoclinic phase and the orthorhombic phases. Where the energy difference for the $Pca2_1$ is $\Delta E_{Pca2_1} = 64 \text{ meV}/f.u.$ (where f.u. is a formula unit) the energy difference for the R3m and R3 phase respectively is $\Delta E_{R3m} = 158 \text{ meV}/f.u.$ and $\Delta E_{R3} = 195 \text{ meV}/f.u.$ according to DFT calculations (see section 2.2 for further explanation). To get the R3m and R3 phases stable one can use doping or put hafnia under mechanical stress [12] [13] [14] [15]. When a R3m/R3 phase hafnia is epitaxially grown as a thin film on a (001)-oriented $SrTiO_3$ the thin film shows properties which are similar to the orthorhombic phases. For thicker films the monoclinic phase coexists with the R3m/R3 phase and this lowers the ferroelectric effects within the thin film. At least for thin films smaller than 10 nm the ferroelectric properties become larger the thinner the thin film is. This is concluded from PUND measurements done by Wei et al., from which the relation between the polarization and the voltage over the thin film can be constructed. For a 9 nm thin film they found a maximal polarization of $P_r = 18 \text{ } \mu\text{C}/\text{cm}^2$ versus a maximal polarization of $P_r = 34 \text{ } \mu\text{C}/\text{cm}^2$ for a thin film of 5 nm thick. The results of the measurements are shown in figure 8. In the figure the typical hysteresis loop of ferro-electric materials is identifiable by the black lines. The blue lines represent the ferroelectric switching currents. The coercive electric field values, the electric field value for which the switching current is maximal, of the two samples, E_c , is approximately $E_c \approx 5 \text{ MV}/\text{cm}$ for the 5 nm sample and $E_c \approx 3 \text{ MV}/\text{cm}$ for the 9 nm sample. The values for the

coercive electric field are to be expected as it follows a $d^{-2/3}$ dependence behaviour.

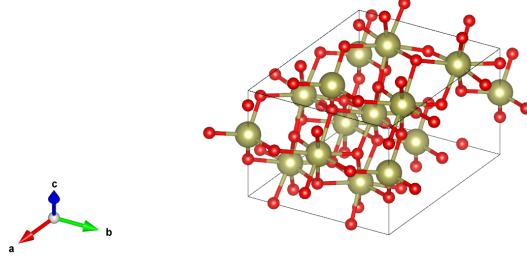


Figure 7: An example of unit cell of the R3m rhombohedral phase of hafnia. Generated using computed data by [8].

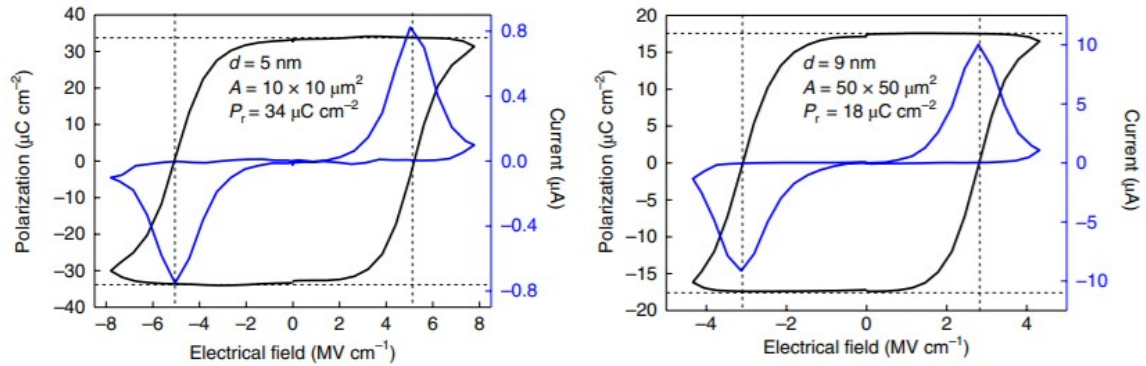


Figure 8: The polarization hysteresis loop of the samples of thin films bei Wei et al. (in black). The switching current is represented in blue. The electric field frequency is $f = 1 \text{ kHz}$ Adapted from [8].

The exact origin of the ferroelectricity in the R3m phase is still to be exactly understood. However, hints were found that a significant part of the ferroelectric behaviour of hafnia, when put under epitaxial strain, can attributed to the bond order of Hf-O bonds. These bonds are alternately longer and shorter than the bond length of Hf-O bonds when the film is not under epitaxial strain [16].

2.2 Phonons and phonon plots

Within thin films all kind of crystals of various elements are present. In turn these crystals are made up of three dimensional lattices with atoms in it [17]. The atoms are bound by potentials to its nearest neighbours such that the potentials can be represented by harmonic oscillator potentials and so the the whole system of the lattice can be represented by harmonic oscillators. Due to

the thermal energy or other potential forces acting on the thin film the atoms may vibrate. This can create a mechanical wave that may travel through the material. Due to periodic boundary conditions on the lattice, the possible energies in the system are definite and quantized [18]. This gives that the mechanical waves throughout the thin films (or any other material) can be described as a quasiparticle. The way how phonons behave within materials depends on the crystal structure of the material. One way to show the dependence of the phonons to the crystal structure is via phonon dispersion relations. A phonon dispersion relation relates the angular frequency of a phonon ω_{ph} or the just the frequency of a phonon f_{ph} to the crystal structure of a material by the wave vector \vec{k} , and so the reciprocal lattice of a material. From the phonon dispersion relation one can for example determine the velocity of the phonon through the material. An example of a phonon dispersion relation of a three dimensional material is shown in figure 9.

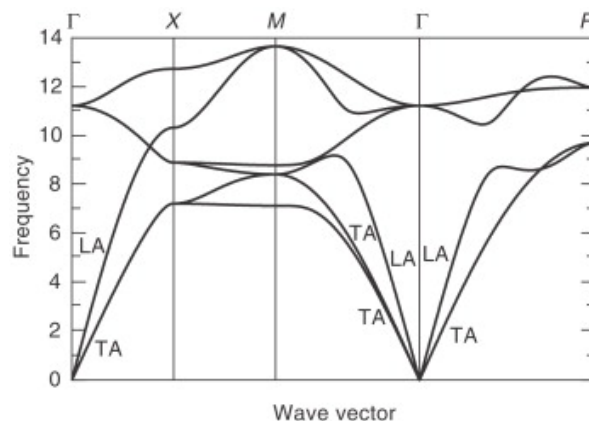


Figure 9: An example of a phonon dispersion relation of a three dimensional material. Adapted from [19].

In a phonon dispersion relation the reciprocal lattice is described by the wave vector \vec{k} . As said before the material lattice is bound by periodic boundary conditions. For the lattice is affected by the periodic boundary conditions so is the reciprocal lattice. Hence the only a certain region within the reciprocal lattice needs to be explored to find the properties of the whole material. This is called the first Brillouin zone [18]. Within the first Brillouin zone there are several high symmetry points and axis. As these points, the paths between them and these axis contain a lot of information about the material, they are the points taken within phonon dispersions to depict. The phonon dispersion relations in figure 9 shows various plots and vertical lines. The vertical lines and the letters above denote the high symmetry points chosen plot. The plot lines, so called branches, denote various modes of oscillation of phonons. The number of branches in a phonon dispersion relation is equal to the number of degrees of freedom that are present in the first Brillouin zone of the material [19]. The Γ -point represents the center of the first Brillouin zone. In every phonon dispersion relation there are three vibrational modes which have a zero frequency at the Γ -point. The vibrational modes which cross $\omega_{ph}(\vec{k}) = 0$ are called the acoustic modes. For these modes neighbouring atoms vibrate in phase. Other vibration modes where the frequency is non-zero at the Γ -point are called optic modes. In these modes neighbouring atoms vibrate in antiphase. For certain crystals with high symmetry along high symmetry directions, as is shown in the phonon dispersion relation of

figure 9, the vibrational modes are polarized. They are either polarized in the direction parallel to the propagation direction of wave vector \vec{k} , or perpendicular to the propagation direction of \vec{k} . These are called the longitudinal and transverse waves respectively. These polarizations apply both to the acoustic and optic modes. Hence in that case there are four possible modes longitudinal acoustic (LA), transverse acoustic (TA), longitudinal optic (LO) and transverse optic (TO). The LA and TA modes are denoted specifically in figure 9.

2.3 Density Functional Theory

To solve the research questions one needs some basic knowledge about Density Functional Theory, DFT in short. DFT is also known by other names such as Ab initio calculations or first principles calculations. Researchers in the (computational) materials science branch of (applied) physics want to know properties of many particle systems like electron density, wave function, and other properties. To examine the properties, one needs to solve the Schrödinger equation [20][21][22]:

$$\begin{aligned} \hat{H}\psi(\{\vec{r}_1, \vec{r}_2, \vec{r}_3, \dots, \vec{r}_N\}, \{\vec{R}_1, \vec{R}_2, \vec{R}_3, \dots, \vec{R}_M\}) &= E\psi(\{\vec{r}_1, \vec{r}_2, \vec{r}_3, \dots, \vec{r}_N\}, \{\vec{R}_1, \vec{R}_2, \vec{R}_3, \dots, \vec{R}_M\}) \\ \hat{H}\psi(\{\vec{r}_i\}, \{\vec{R}_I\}) &= E\psi(\{\vec{r}_i\}, \{\vec{R}_I\}) \end{aligned} \quad (1)$$

In equation 1 \hat{H} stands for the Hamiltonian operator, E for the energy in the system. $\psi(\dots)$ for the many-particle wave function, r , the spatial position of an electron, N the number of electrons, R the spatial coordinate of a nucleus in the system and M the number of nuclei in the system. i and I are indices for respectively the electrons and the nuclei. Letting the Hamiltonian operator for what it is now, one can see that for large systems of atoms or molecules the number of degrees of freedom in the system might become very large, $3N + 3M$, referring to the three spatial coordinates per electron/nucleus. With that the many-particle wave function also becomes very complicated. For such large systems it is (almost) impossible to analytically compute the wavelength solution and also computationally, as the computational load becomes immensely large very quickly with systems becoming larger. To be able to actually compute the properties of the system, one needs to apply some approximations to simplify the problem. The first approximation one can apply is the Born-Oppenheimer approximation. The nuclei in systems can be assumed to have a much larger (effective) mass than the electrons, $m_n \gg m_e$. This results in a situation that the electrons can move around much easier than the nuclei so the the nuclei are almost static with respect to the fast moving electrons. Hence one can decouple the dynamics of the nuclei and the electrons which results to the following:

$$\psi(\{\vec{r}_i\}, \{\vec{R}_I\}) = \psi_e(\{\vec{r}_i\}) \cdot \psi_n(\{\vec{R}_I\}) \quad (2)$$

We can now independently apply the Hamiltonian to the 'many-electron' wave function and the 'many-nucleus' wave function. To further simplify the problem one can assume any electron (or nucleus) in the system to be a point charge in the field of all the other electrons (or nuclei). This further simplifies the problem in terms of the Hartree product:

$$\psi_e(\{\vec{r}_i\}) = \psi_{e,1}(\vec{r}_1) \cdot \psi_{e,2}(\vec{r}_2) \cdot \dots \cdot \psi_{e,N}(\vec{r}_N) \quad (3)$$

$$\psi_n(\{\vec{R}_I\}) = \psi_{n,1}(\vec{R}_1) \cdot \psi_{n,2}(\vec{R}_2) \cdot \dots \cdot \psi_{n,M}(\vec{R}_M) \quad (4)$$

Equation 3 represents the electron version and equation 4 the nucleus version. The many-electron and many-nucleus wave equations have now changed to a many one-electron wave function and a many one-nucleus wave function. Using these two approximations it becomes easier to compute the final wave function as a whole. As the nucleus part of the wave equation can be solved analogous to the electron part, lets now focus on the electron part of the wave function. Lets now look at the Hamiltonian. Let's presume that the wave function is time-independent and we can use the time-independent Schrödinger equation. It is in the case of this kind of system equal to

$$\hat{H} = -\frac{\hbar}{2m_e} \sum_i^N \nabla_i^2 + \sum_i^N V_Z(\vec{r}_i) + \frac{1}{2} \sum_i^N \sum_{i \neq j} U(\vec{r}_i, \vec{r}_j) \quad (5)$$

In equation 5 \hbar is the constant of Dirac, V_Z the external potential the electrons feel (due to the various nuclei) and $U(\vec{r}_i, \vec{r}_j)$ the Coulomb potential. The first term in the equation determines the kinetic energy of the electron, the second term the attraction potential between the nuclei and the electron and the third term the Coulomb potential that describes the repulsion potential between the electron and a specific other electron in the system when applying the Hamiltonian onto a wave function. Every term summed up determines their contribution to the total energy in the system. Equation 4 and 5 both depend on the spatial coordinates of all the electrons in the system. To shrink the degrees of freedom in the system, we can define the electron density. It is defined as follows:

$$\rho(\vec{r}) = \sum_i^N |\psi_e(r_i)|^2 \quad (6)$$

Equation 6 changes the degrees of freedom from $3N$ to 3. This would change the computational load by a lot, if it were not for the fact that the Hamiltonian is in no way dependent on the electron density. However, here we can make use of Hohenberg-Kohn-Sham DFT. Firstly, Hohenberg, Kohn and Sham proved that there exists a unique functional dependent on the electron density that is equal to the ground state energy a system. In other words: $E = E[n(\vec{r})]$. They further worked it out to the following equation:

$$E[\rho] = K[\psi(\rho)] + E_Z[\rho] + E_C[\rho] + E_{ion} + E_{XC} \quad (7)$$

$$E[\rho] = -\frac{\hbar}{m_e} \sum_i \int \psi_{e,i}^* \nabla^2 \psi_{e,i} d^3r + \int V(\vec{r}) \rho(\vec{r}) d^3r + \frac{e^2}{2} \iint \frac{\rho(\vec{r}) \rho(\vec{r}')}{|\vec{r} - \vec{r}'|} d^3r d^3r' + E_{ion} + E_{XC} \quad (8)$$

Equation 7 gives the simple relation Hohenberg, Kohn and Sham derived. They stated that the total energy in the system is equal to the sum of the kinetic energy (first term), the attraction energy between the nuclei and the electrons (second term), the Coulomb repulsion energy between the electrons (third term), the energies in the system due to the nucleus-to-nucleus repulsion (fourth term) and the so called exchange correlation energy. The first four energies are known and can be computed (with various difficulty). They are worked out in equation 8, with the exception of the nucleus-to-nucleus repulsion term as we are focusing on electrons at the moment. But if one wants to the term can be merged into the Coulomb term by redefining the electron density for the Coulomb term by $\rho_{eZ}(\vec{r}) = \rho(\vec{r}) + \sum_i Z_i \delta(\vec{r} - \vec{R}_i)$ where Z_i is the charge of the one of the nuclei in the system and $\delta(\dots)$ the delta function. The exchange correlation energy term is responsible for the energy

which can be attributed to quantum mechanical effects in the system. The exchange correlation energy is in contrast to the other terms unknown. There is no analytical expression for the exchange correlation energy. However, the exchange correlation energy can be approximated. The exchange correlation energy can be modeled by the uniform electron gas (UEG) with some approximations. These exchange correlation electron density functionals are known as for the UEG the energies have been computed through Monte-Carlo simulations for a vary wide range of electron densities. If they are parametrized, they yield density functionals. The approximations done one the UEG are generally the local density approximation (LDA) which just states that an inhomogeneous electron gas, the material/system in question, is locally approximated to be homogeneous and the General Gradient Approximation (GGA) which next to the LDA takes the local gradient of the electron density into account. As the exchange correlation energy now is known for the core electrons, only the exchange correlation energy for the valence electrons needs to be computed in simulations. Now that all the individual terms of equation 7 are known or can be derived we can look at the following. The Hamiltonian operator can be rewritten such that it can form the Kohn-Sham equation:

$$\left(-\frac{\hbar}{2m}\nabla^2 + V_Z[\rho](\vec{r}) + V_C[\rho](\vec{r}) + V_{XC}[\rho](\vec{r}) \right) \psi_{e,i}(\vec{r}) = \epsilon_{e,i} \psi_{e,i}(\vec{r}) \quad (9)$$

$$\left(-\frac{\hbar}{2m}\nabla^2 + V_C[\rho_{eZ}](\vec{r}) + V_{XC}[\rho](\vec{r}) \right) \psi_{e,i}(\vec{r}) = \epsilon_{e,i} \psi_{e,i}(\vec{r}) \quad (10)$$

Equation 9 shows the full out written Kohn-Sham equation and equation 10 the version where a version in which the nuclei repulsion term is taken into the Coulomb repulsion term. In both equations $\epsilon_{e,i}$ is the total energy belonging to the wave function $\psi_{e,i}$. The number of degrees of freedom in the Kohn-Sham equation is just 3, so this greatly reduces the computational load of computation with respect to the Schrödinger equation. Next to proving that there exists a unique functional which relates the energy of a system to the electron density Hohenberg, Kohn and Sham also found that minimizing the overall functional which relates the energy in the system to the electron density also results in finding the true ground state electron density of the system. This makes a process possible to determine the true ground state electron density and doing so all the other determinable properties (via the Hamiltonian) in the system. The scheme is can is shown in figure 10.

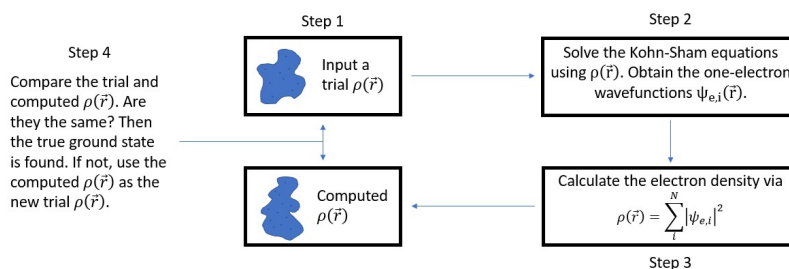


Figure 10: The scheme to determine the true ground state of a many-particle system using DFT. Reproduced using information from [20].

As the scheme in figure 10 shows, to find the true ground state in the system a trial electron density is needed. To accurately find the true ground state of a system one needs an $n(\vec{r})$ that is a good

initial guess. These initial guesses might vary from situation to situation. Usually software used to do DFT calculations have very good initial guesses built into them. Next to the approximations done on the wave function and the Hamiltonian, there are some further simplifications which are applied in DFT PAW orbitals, etcetera. However, these go very deep into the theory behind DFT but the software used in this thesis project accounts for it perfectly.

3 Methods and setup

In this section an introduction to VASP, the many-particle system simulator that is used for this thesis project, is given. Furthermore the methods describing the use of VASP on how to answer the research questions will be explained.

3.1 Introduction to VASP

VASP, the Vienna Ab initio Simulation Package, is a software package by which DFT calculations and simulations can be performed [23][24][25][26][27]. VASP provides the tools to answer the reasearch questions. The VASP software runs on a university-run Ubuntu server. VASP is managed in Ubuntu by the Slurm workload manager. Jobs can be submitted to the Slurm workload manager by job scripts. An example of a job script can be seen in figure 11. Depending on the resources available to the server the submitted job script may be lined up in a queue before execution starts on VASP.

```
#!/bin/bash
#SBATCH -t 72:00:00
#SBATCH -p bigmem
#SBATCH -N 2 --tasks-per-node=8
#SBATCH --output=R3m.out
#SBATCH --error=R3m.err
#SBATCH --mail-type=all
#SBATCH --exclusive
#SBATCH --mail-user=[REDACTED]utwente.nl
module load compiler/intel/13.1.117
module load mkl/11.0.1
module load mpi/intel/4.1.0.024
module load mpi/openmpi/1.7.4
module load fftw/3.3.3
ulimit -s unlimited
cd $PWD
srun [REDACTED]/vasp/vasp5.3
```

Figure 11: A very typical example of a job script that can be submitted to slurm. Some info has been painted out to protect the privacy of the persons involved in the making of this specific job script.

Various parameters can be set in the job script that can influence the VASP simulation (The lines with parameters are preceded by #SBATCH). A couple of important parameters cat be set. They are following:

- **-t**: Determines the maximum time that a job is allowed to run. This is an important property to set to prevent infinite duration of erroneous simulations. For simulation length vary with the computational load of the simulation, this duration needs to be updated regularly.
- **-p**: Determines the partition on which the job will be performed.
- **-N**: Determines the number of nodes the simulation should run on. On the Ubuntu server the number of nodes available is limited to a number of eight.

- **-output=...** / **-error=...** These parameters determine the filepath where the output and/or error document should be generated. They also control the name of the generated document and the document extension

Other parameters include the possibility to assign a specific number of tasks to a node and to send notifications about the specific job when it is run to a certain email address. The lines after the parameters load some modules needed for VASP to run and a command to run VASP. The output (document) of the VASP software contains all the information needed to the energy values of systems and the polarization values of systems. For phonon dispersion relations also the program Phonopy needs to be used together with VASP. VASP has five different input files: POSCAR, INCAR, KPOINTS and POTCAR. These are all text files. They all have different uses:

- **POSCAR:** The POSCAR file gives the input lattice and material to VASP that it has to process in the simulation [28]. An example of a typical POSCAR file can be seen in figure 12. Within the example the first line just is a arbitrary name the author can give the text file. The second to the fifth line specifies the spatial layout of the unit cell with the third to fifth line representing the cartesian coordinates of the \vec{a} , \vec{b} and \vec{c} lattice vectors respectively. The second line defines a scaling vector to the lattice vectors. The sixth and seventh line specify the type of atoms that is used in the simulation and the number of them. Line eight to the last line refer to the position of the atoms within the unit cell. The tag direct means the positions are given relative to the lattice vectors. The tag can be changed to cartesian to express the atom positions in cartesian coordinates. There is an extra tag that can be used called selective dynamics. Using this tag directly after the seventh line makes it possible to, for relaxation simulations, fix the positions in a specific lattice vector direction so that they are not allowed to relax.

```
Hf4 O8
1.0
5.069186 0.000000 -0.864173
0.000000 5.195148 0.000000
0.000000 0.000000 5.326038
Hf O
4 8
direct
0.724041 0.542681 0.292109 Hf
0.275959 0.042681 0.207891 Hf
0.275959 0.457319 0.707891 Hf
0.724041 0.957319 0.792109 Hf
0.551113 0.257397 0.022292 O
0.448887 0.757397 0.477708 O
0.448887 0.742603 0.977708 O
0.551113 0.242603 0.522292 O
0.932151 0.669878 0.652906 O
0.067849 0.169878 0.847094 O
0.067849 0.330122 0.347094 O
0.932151 0.830122 0.152906 O
```

Figure 12: An typical example of a POSCAR file, in this case of unit cell containing 4 units of hafnia. In this example hafnia is in the P2₁/c phase.

- **INCAR:** The INCAR file makes it possible to set various parameters for the simulations done in vasp [29]. An example of an INCAR text file can be seen in figure 13. The most important parameters are EDIFF (sets a break condition for the convergence of the minimum energy in eV), ENCUT (specifies the maximum plane wave energy taken into consideration within the simulation to solve the Kohn-Sham equation), IBRION (specifies the mode in which the simulation has to run and with which algorithm, ISIF (specifies if the stress tensor is computed in simulations and assigns degrees of freedom to atom positions, the cell shape and its volume), NELM (Specifies the maximum number of self-consistency steps during an ionic step), NSW (Specifies the maximum number of ionic steps during a simulation) and LCALCPOL (switches the evaluation of the Berry phase expressions on or off for the calculation of the polarization in a sample). The other parameters are important but are constant throughout all of the simulations and require significant knowledge of the software. The parameters have to be set correctly or otherwise this may lead to the simulation being unstable and producing unphysical simulation results.

```

ALGO = Fast
EDIFF = 0.00060000000000000001
ENCUT = 520
IBRION = 2
ISIF = 3
ISMEAR = -5
ISPIN = 1
LORBIT = 11
LREAL = Auto
LWAVE = False
NELM = 100
NSW = 99
PREC = Accurate
SIGMA = 0.05
LCALCPOL = .TRUE.

```

Figure 13: A typical example of an INCAR file with parameters set for a simulation.

- **KPOINTS:** To run the simulations in VASP, a large number of integrals need to be performed over the first Brillouin zone. To sample the first Brillouin zone correctly there are several options in VASP. These are set in the KPOINTS file [30]. An example of a KPOINTS textfile can be viewed in figure 14. The first line just is a document title freely changeable by the user. The second line sets the number of sampling points in the reciprocal lattice. If a zero is denoted there, VASP itself generates a mesh with sampling points for the reciprocal lattice, like is the case in the example KPOINTS text file. There are three different algorithms for the automatic mesh generation. The algorithm used for all of the research in this thesis is the Monkhorst-Pack algorithm (denoted by 'Monkhorst' on the third line of the example file), which is a mesh generation algorithm centered around the Γ -point in reciprocal space. The fourth line in the file specifies subdivisions of the to be generated mesh along the reciprocal lattice vectors.

```

pymatgen v2019.10.16 with grid density = 1358 / atom
0
Monkhorst
4 4 4

```

Figure 14: An example of an KPOINTS file with the parameters for the sampling of the reciprocal lattice in the simulation.

- POTCAR:** To perform the simulations the Kohn-Sham equation needs to be solved using plane waves. However, for almost all of the materials, except for materials with a very small atomic number, this is not possible [22]. This is due to spatial strongly localized states of the wave function and/or due to rapid oscillations of orbitals near the nucleus. Two approximations are done to combat this. As the properties of materials/systems are for almost all cases only dependent on the valence electrons of atoms one can use the frozen core approximation. For real calculations only the valence electrons are able to move, the 'core' electrons are frozen on their place and their properties are pre-calculated. Furthermore to fix the rapid oscillations near nuclei of materials, VASP uses pseudopotentials. An example of a pseudopotential can be seen in figure 15. For bonding of atoms only a certain range above a certain threshold of the wave function is of interest as the bonding never takes place below this threshold. The threshold in figure 15 is r_c . As the rapid oscillations are (almost) always below r_c as they are close to the nucleus, one does not care for them, but the full wave function is required for the calculation. Hence VASP smoothes out the rapid oscillations of the wave functions below r_c by altering the potential V to \tilde{V} and with that the corresponding wave function from ψ to $\tilde{\psi}$. The information related to the frozen core approximation and the pseudopotentials are stored in the POTCAR text file [31]. POTCARs are available per material in a catalog provided by VASP. An example of a POTCAR is not shown here due to copyright resting on all POTCARs provided by VASP.

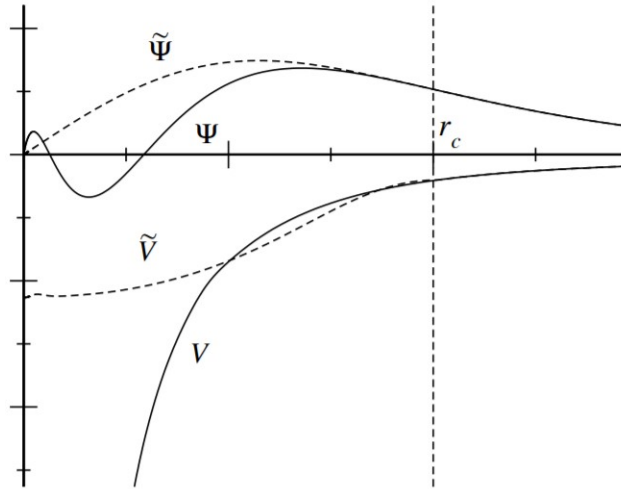


Figure 15: A normal potential and wave function corresponding to an orbital, V and ψ , and the corresponding pseudopotentials, \tilde{V} and $\tilde{\psi}$.

3.2 Retrieving energy values

To find the energy values corresponding to the various phases of hafnia one wants to use VASP to the ground state energy of such a state. The method VASP uses to determine the ground state energy is depicted in the scheme in figure 10. To do so we want to make use of the ionic relaxation mode of VASP, which searches for a local minimum energy given the input. The simulation takes place at a temperature $0K$ and is assumed to run in vacuum. First we need to supply VASP with the POSCARs of the all of the phases where ionic relaxation will be applied to. The following phases will be simulated: Fm-3m, P2₁/c, P4₂/nmc, P4₂/mmm, Pbca, Pbcn, Pbca2₁, Pmn2₁, Pmna and R3m-Bulk. For all phases except the R3m ones the POSCARs are retrieved from 'The Materials Project', an open-access database which offers POSCARs as well as various material properties for a wide range of materials [10] [32]. The POSCARs for the R3m phases are generated using structure information of the R3m phases from the supplementary material of the paper by Wei et al. [8] by the STRCONVERT function of the Bilbao Crystallographic Server [33] [34]. The R3m-strained phase is in accordance with thin film growth of hafnia on SrTiO₃. Next to giving the structure information via the POSCARs to VASP, tags in the INCAR file need to be set. Firstly IBRION needs to be set to 2. This sets VASP up such that it will use the conjugate gradient algorithm to accomplish ionic relaxation [35]. Furthermore ENCUT needs to be set. The value for the non-R3m phases will be set to $520eV$, as this is in accordance with the simulations done on these phases by The materials Project. For the R3m phases this is set to $500 eV$, in accordance with the DFT simulations done by Wei et al. ISIF is set to three for all phases, which gives the atoms, the cell shape and cell volume degrees of freedom. This means that all the called properties are allowed to change in value. EDIFF is for the non-R3m phases either $6 * 10^{-4} eV$ or $3 * 10^{-4} eV$. This is according to the EDIFF value for the simulations by The Materials Project. Wei et al. did not use the EDIFF tag for a global break condition. Via the tag EDIFFG they set the global break condition as a force [36]. The global break condition is met if the norm of the force acting on all the atoms in the system is smaller than a force of $0.005 eV/\text{\AA}$. This is then also the tag and setting that will be used for the simulations. For all simulations NELM is set to 100 and NSW to 99. LCALCPOL is set to false as for these simulations there is set to false, as there is no interest yet in researching the polarization of the phases of hafnia. The KPOINTS file in all cases uses an automated generated mesh to sample the first Brillouin zone with the Monkhorst-Pack algorithm. The number of subdivisions differs per phase but is in accordance with the settings used for simulations by The Materials Project. The POTCARs for oxygen and hafnia are retrieved from the VASP catalogue (for hafnia specifically Hf_pv as it is used for simulations by The Materials Project) in the Local Density Approximation. To make sure that the energy values that will be found for the phases are correct or are at least of the same order of magnitude the energy values will be compared to the energy values computed in [8] and [9]. This method will be used for all of the three research questions.

3.3 Computing phonon dispersion relations

To compute phonon dispersion relations with VASP one needs to use another mode. The mode which is needed now is the second derivatives/Hessian matrix mode. Using this mode VASP will simulate vibrations of all of the atoms in all cartesian directions [35]. With the information VASP retrieves from the simulation it can compute the Hessian matrix, the needed quantity to compute the phonon dispersion relations for all the different phases. The POSCARs for the computation of the Hessian matrix are the same as the ones for retrieving the energy values. The INCARs also almost stays the same. One tag need to be changed to change the mode of VASP and to make

sure that the simulation becomes instable and that results become unphysical. To make sure that the simulation will remain stable, the tag EDIFFG should not be used with a negative value, which sets the global break condition to a situation where the norm on the forces on all the atoms in the simulation is smaller than a certain value. To change the mode to the second derivatives/Hessian matrix mode IBRION is set to 8. Furthermore the following tags and values are set: LREAL = .FALSE. , ADDGRID = .TRUE. and LCHARG = .FALSE. . All the other tags stay constant with respect to the situation of section 3.2. The same goes for the KPOINTS and the POTCAR. There is not a lot of room for experimentation with settings as the Hessian matrix simulations take a lot of computing power and one simulation can easily take a couple of days. After the Hessian matrix is computed one can use another piece of software to compute the phonon dispersion relations. VASP cannot generate the phonon dispersion relations itself. This piece of software is called Phonopy. Given the Hessian matrix from VASP and a route it should display throughout the reciprocal lattice Phonopy is able to produce the phonon dispersion relations [37]. The Hessian matrix is easily passed over to Phonopy. The route description throughout the reciprocal lattice is another story however. One wants the route to follow the high-symmetry points and high-symmetry lines. The point with the highest symmetry is the Γ -point, so it is included in all phonon dispersion relations. To select the other points and paths the Bilbao Crystallographic Server is used again [33] [34]. Specifically the function KVEC, which makes it possible to view the reciprocal lattice of all included phases and with that given the coordinates of high-symmetry points. This way a path between the high-symmetry points can be mapped out. For the simulations the routes are laid out through the reciprocal lattice in such a way that the phonon dispersion relations are comparable to work done by Huan et al. [9]. To verify the validity of the phonon dispersion relations they are compared to the ones computed by Huan et al. These can be found in the supplementary material of [9]. The phases of Fm-3m, P2₁/c, Pbca, Pnma, P4₂/nmc, Pca2₁ and Pmn2₁ can be compared. For the R3m-phases no comparison material is found in the literature. For the R3m-phases it is important to notice that depending on the length of the \vec{a} and \vec{c} lattice vectors the Brillouin zone changes, according to the Bilbao crystallographic server. The Brillouin zone phase transition point occurs at

$$\sqrt{3|\vec{a}|} = \sqrt{2|\vec{c}|} \quad (11)$$

If the to be compared phases can be produced within reasonable accuracy, phonon dispersion relations of the R3m phases may give valuable information about instabilities in the R3m phases through negative frequencies showing up. This method will be used to answer the first two research questions.

3.4 Epitaxially strained hafnia

To further answer the research questions two extra phases are introduced to the simulations: R3m-ES-GaN and R3m-ES-SrTiO₃, the R3m phase of hafnia grown on a substrate of respectively GaN and SrTiO₃. Wei et al. researched the R3m-phase to be grown as a thin film on a substrate of SrTiO₃. However, for IMS it is of interest to have the R3M phase of hafnia epitaxially strained on a substrate of GaN, Gallium nitride. By adding them the energy levels of the phases and the phonon dispersion relations can be computed, as well as the possible polarization of the phase, with respect to the other two R3m phases. Furthermore an intermediate phase between R3m-ES-SrTiO₃ and R3m-ES-GaN is created to look if the interpolation of lattice vectors gives an interesting phonon dispersion relation. That phase is denoted by R3m-ES-int. First the energy level. To do all the

calculations on R3m-ES-GaN one just can copy the POSCAR from R3m-ES-SrTiO₃. The only minor correction one needs to make is that the \vec{a} and \vec{b} lattice needs to be changed so it fits a epitaxially strained situation on GaN. Both hafnia in the R3m phase and the stable P6₃mc phase of GaN are rhombohedral. To strain the R3m hafnia phase \vec{a} and \vec{b} can be changed to the length of the same lattice vectors of GaN in the P6₃mc phase. This means that that the specific lattice vectors will be changed such that they have a length of 6.432 Å. This is twice the length of the \vec{a} and \vec{b} lattice vector of the primitive unit cell, as the unit cell in the VASP simulations is eight times larger [10] [32]. Via this way the hafnia is (001) oriented on the substrate, which is not the case for the research done by Wei et al. [8], as there the hafnia is (111) oriented on the substrate. This is to done to keep the simulation simple, as in case of a (111) oriented R3m-hafnia phase the geometry becomes more complex. It is not totally clear how the \vec{c} lattice vector would react to the sudden change of the \vec{a} and \vec{b} . One would want to let \vec{c} relax and find the minimum energy. VASP itself does not allow for relaxation of one specific lattice vector. To solve this one can let VASP perform multiple ionic relaxation simulations, like in 3.2, while changing \vec{c} per run to find the energy profile of R3m-ES-GaN as a function of the length of the \vec{c} lattice vector. This is possible by changing the job script and running VASP in a loop. The change of the standard job script is shown in Appendix A. As a starting point for searching for the minimum energy one could assume volume conservation and via that compute the expected length of the \vec{c} lattice vector. For R3m-ES-GaN this gives an expected \vec{c} lattice vector length of 10.5 Å. To create some material for comparison and validation, this procedure is also followed with the R3m-ES-SrTiO₃ and R3m-Bulk phase. The expected \vec{c} lattice vector length during these simulations the polarization values of the phases as a function of the \vec{c} lattice vector is also saved for analysis. If the optimized structure is found, then phonon dispersion relations can be computed as in subsection 3.3 and R3m-ES-int can be made by interpolation of the POSCARs of R3m-ES-SrTiO₃ and R3m-ES-GaN. In turn then also a phonon dispersion relation can be computed and analyzed of R3m-ES-int. This method will be used to answer to last two research questions.

4 Results

In this section the results of the research will be presented, in the order of the research questions.

4.1 Reproduction of past research

4.1.1 Energy values of the hafnia phases

Using VASP and Phonopy the energy values all of the researched phases of hafnia could be computed. Due to computational problems in VASP the phonon dispersion relations of the Pbcn phase of hafnia could not be computed. VASP was not able to converge to an energy value to compute the Hessian matrix in that case. This is likely due to the POSCAR needing 288 atoms in the unit cell for the simulation, with respect to at maximum 96 atoms for the other phases. VASP probably cannot handle a unit cell with such a large number of atoms. The computed energy values of the phases of hafnia can be found in table 1.

	P2 ₁ /c	Fm-3m	Pbca	P4 ₂ /nmc	Pmn2 ₁	Pca2 ₁
Energy values of the phases in eV/f.u.	-33.2452	-33.0765	-33.2195	-33.1320	-33.1380	-33.1931
Energy difference with P2 ₁ /c in meV/f.u.	0	168.7	25.7	113.2	107.2	52.1
Energy difference with P2 ₁ /c in meV/atom	0	56.2	8.6	37.7	35.7	17.4

	P4 ₂ /mnm	Pnma	R3m-Bulk
Energy values of the phases in eV/f.u.	-33.0130	-33.0414	-33.1113
Energy difference with P2 ₁ /c in meV/f.u.	232.2	203.8	133.9
Energy difference with P2 ₁ /c in meV/atom	77.4	67.9	44.6

Table 1: The computed energy values per phase of hafnia.

Before doing any comparisons direct one can notice that directly that the P2₁/c has the lowest energy. According to Wei et al. [8] and Huan et al. [9] this should be the case as the simulation is run at 0 K and in vacuum. The difference in energy between the stable phase and the other phases of hafnia according to Huan et al. and Wei et al. stand in table 2.

	P2 ₁ /c	Fm-3m	Pbca	P4 ₂ /nmc	Pmn2 ₁	Pca2 ₁
Energy difference with P2 ₁ /c in meV/f.u. [8]	0	-	-	-	-	64
Energy difference with P2 ₁ /c in meV/atom [9]	0	-	~ 22	~ 59	~ 56	~ 23

	P4 ₂ /mnm	Pnma	R3m-Bulk
Energy difference with P2 ₁ /c in meV/f.u. [8]	-	-	158
Energy difference with P2 ₁ /c in meV/atom [9]	-	>>60	-

Table 2: The computed energy values per phase of hafnia by Wei et al. and Huan et al.

What can be noted firstly is that the computed energy differences and the reference energy values from the literature are in all cases of the same order of magnitude. The minimum difference between the energy differences by Huan et al. is 6 meV/atom and the maximum 21 meV/atom . This hints to the fact that some other approximations have been used. Huan et al. did not use VASP but ABINIT to perform their DFT calculations. For this research the local density approximation was used, but Huan et al., just as Wei et al., used the Perdew-Burke-Ernzerhof approximation, a form of general gradient approximation. Huan et al. furthermore used a different value for ENCUT. They set an equivalent setting in ABINIT to 1000 eV. One or more approximations might have been the cause for these deviations, but it might also have been due to another cause. The error in simulations might also be a possible cause of the deviations. The same goes for the differences in the energy differences by Wei et al. There the maximum is 24 meV/f.u. . To state that the computed energy levels are accurate enough is difficult to say, as these computations never can fully represent reality, but with respect to the literary energy values one could conclude that they are a rough approximation.

4.1.2 Phonon dispersion relations of the hafnia phases

As for the phonon dispersion relations, in a first round of simulations most of the simulations were unstable and they produced mostly unphysical results. Such an unphysical result is shown in figure 16. As one can see a lot of branches with negative frequencies are shown. Normally negative frequencies are not possible, but they are in phonon dispersion relations. Negative frequencies in a phonon dispersion relation hint a permanent displacement of atoms around a point, which might cause ferroelectric properties to show up. However, these branches negative frequencies are usually not that frequent as in figure 16. They are very negative, twice as negative with respect to what is possible in stable hafnia phases, and there are a lot of them. In the phonon dispersion relations of stable hafnia only one or at most two of three branches go into the negative domain. Additionally, there are branches that are stay negative over the whole domain. This is not seen in all of the stable phonon dispersion relations. Next to the negative branches, it is very clear that there are no acoustical branches going through the Γ -point with a zero frequency. One would expect to at least three acoustic branches. Taking everything in account one can conclude that phonon dispersion relations like the one in figure 16 is unphysical.

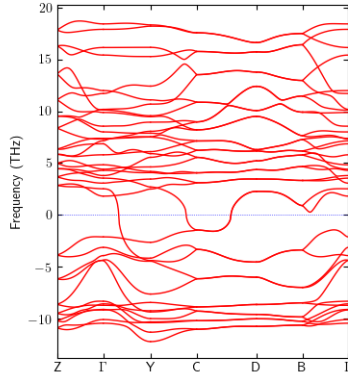


Figure 16: The unphysical phonon dispersion relation after an unstable simulation run of $P2_1/c$.

For a second round of simulations, no unphysical phonon dispersion relations were found. This is due to the fact that the EDIFFG tag with a negative value was removed from all the INCARs, which was used in the first run to test the setting. The phonon dispersion relations that can be compared to the material by Huan et al. [9] are comparable to their counterparts. As said the computed dispersion relations are physical and furthermore they compare to the phonon dispersion relations that are computed by Huan et al., except for The Fm-3m hafnia phase is an exception to the upper . That phase does seem to produce physical results given the acoustic branches, but is not comparable to the research by Huan et al. All of the comparable phonon dispersion relations are shown below.

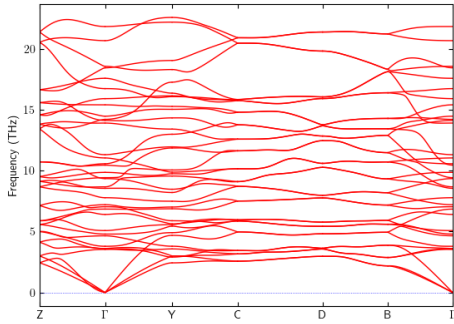


Figure 17: The computed phonon dispersion relation for the $P2_1/c$ phase of hafnia.

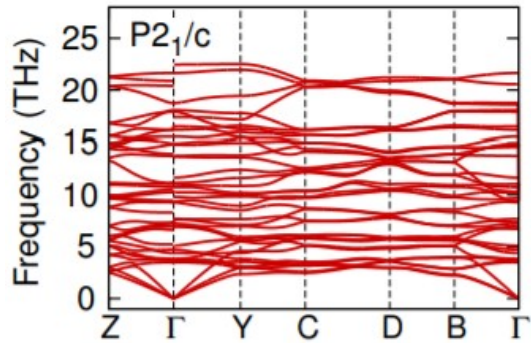


Figure 18: Phonon dispersion relation for the $P2_1/c$ phase of hafnia. Adapted from [9].

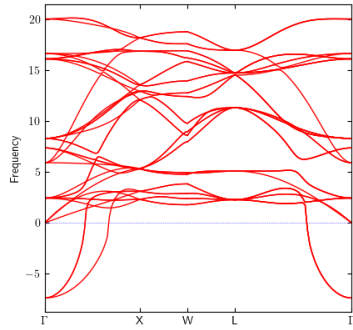


Figure 19: The computed phonon dispersion relation for the Fm-3m phase of hafnia.

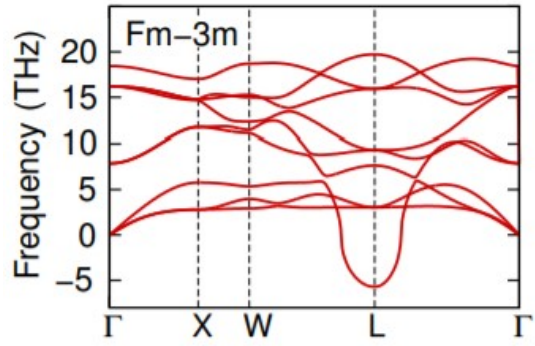


Figure 20: Phonon dispersion relation for the Fm-3m phase of hafnia. Adapted from [9].

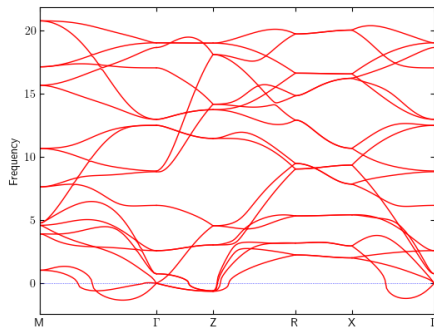


Figure 21: The computed phonon dispersion relation for the P4₂/nmc phase of hafnia.

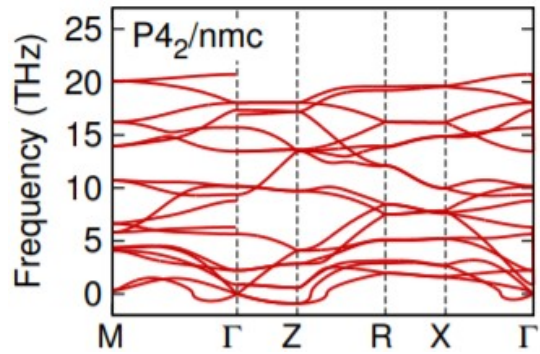


Figure 22: Phonon dispersion relation for the P4₂/nmc phase of hafnia. Adapted from [9].

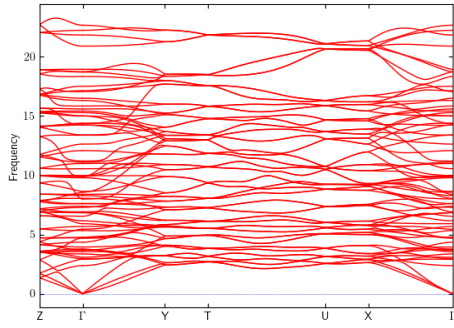


Figure 23: The computed phonon dispersion relation for the PbcA phase of hafnia.

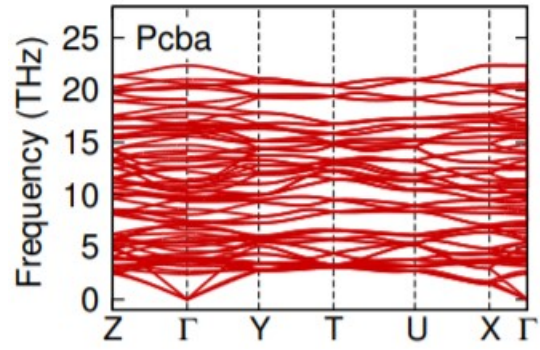


Figure 24: Phonon dispersion relation for the PcbA phase of hafnia. Adapted from [9].

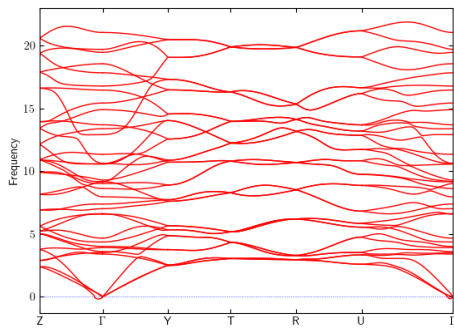


Figure 25: The computed phonon dispersion relation for the Pca₂₁ phase of hafnia.

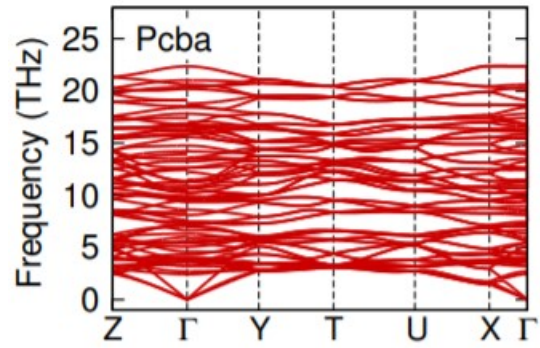


Figure 26: Phonon dispersion relation for the PcbA phase of hafnia. Adapted from [9].

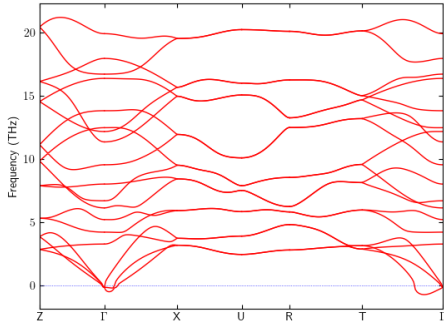


Figure 27: The computed phonon dispersion relation for the $Pmn2_1$ phase of hafnia.

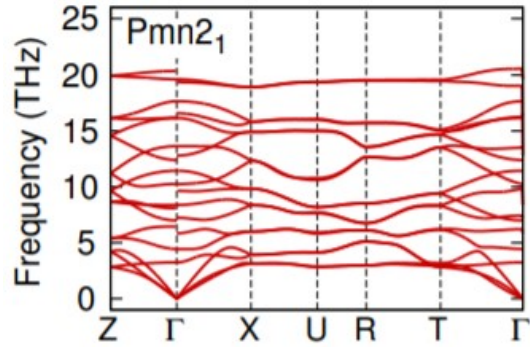


Figure 28: Phonon dispersion relation for the $Pmn2_1$ phase of hafnia. Adapted from [9].

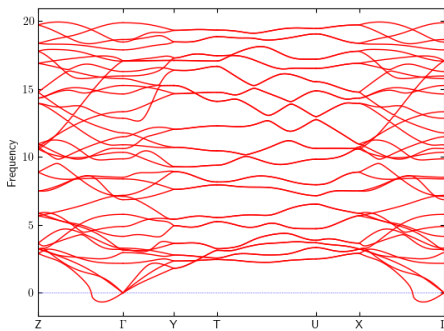


Figure 29: The computed phonon dispersion relation for the $Pmna$ phase of hafnia.

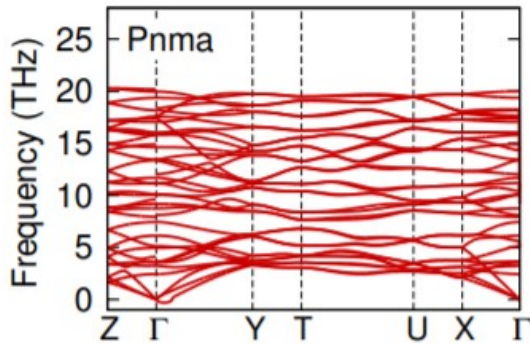


Figure 30: Phonon dispersion relation for the $Pmna$ phase of hafnia. Adapted from [9].

The computed phonon dispersion relations in the upper figures from the second run do represent physical situations. In all cases there are three acoustic branches and there are no branches that stay negative over the whole domain of the phonon dispersion relations. What strikes about the literary phonon dispersion relations is that for some of them there are branches that are discontinuous at Γ . That should not be possible as it is not possible for the phonons cannot take multiple values at a certain point. The branches of the computed phonon dispersion relations are all continuous around Γ . The computed phonon dispersion relations all follow the same patterns as their literary counterparts except for the $Fm-3m$ phonon dispersion relations in figure 19 and 20. In case of the $Fm-3m$ phase some of the all-positive frequency branches follow the same patterns over the whole domain regardless of which version of dispersion relation you look at. However what is clearly visible is that the negative branches in the computed one are in the region around Γ and for the literary one around L . It is not clear what the origin of this discrepancy is. As there are only respectively two and one branch(es) that become(s) negative over some part of the domain this is not likely due to

an error, more like a difference in approximations. Either way the negative branches suggest some atoms might be permanently displaced, which might also make that there will be a phase-change. This plays especially for the computed phonon dispersion relation as there the negativity centers around Γ , which is a high-symmetry point so a change to atom position at Γ directly changes the (degree of) symmetry of the normal lattice. For both the computed and literary phonon dispersion relations for the $P4_2/nmc$ phase of hafnia there are small negative frequency dips around Γ and Z . This is not a surprise as the $P4_2/nmc$ phase is described as the parent phase of the ferroelectric $Pmn2_1$ and $Pca2_1$ so atom displacement around the Γ point is to be expected [9]. The computed phonon dispersion relations of $Pbca$ and $Pmn2_1$ do show very small negative frequency dips of branches round the Γ point. Next to the fact that the dips are very small they are not found back in their literary counterparts, so they are probably just due to computational errors. Both the computed and literary phonon dispersion relations of the $Pnma$ phase of hafnia do show negative frequency dips of branches around Γ . They are larger than the frequency dips in the computed dispersion relations of the $Pbca$ and $Pmn2_1$ phases, about of the other of the negative frequency dips of the $P4_2/nmc$ phase. This hence might point to a symmetry change of the real lattice. In conclusion, as the computed phonon dispersion relations follow the same patterns as their literary counterparts to a high degree, with the exception of the $Fm-3m$ phase, the simulations by VASP are a good approximation for a computational prediction of the real phonon dispersion relations of the $R3m$ -phases.

4.2 Energy values and phonon spectra of the $R3m$ phase of hafnia on GaN

As concluded in subsections 4.1.1 and 4.1.2 both for the energy values and the phonon dispersion relations the computed ones form a good approximation and so can with reasonable accuracy be used to compute them for the $R3m$ phase of hafnia in different conditions. Firstly the energy values. The simulations in VASP of the two phases described by Wei et al. [8] retrieve the following energy values:

	R3m-Bulk	R3m-ES-SrTiO ₃
Energy values of the phases in eV/f.u.	-33.1113	-33.1087
Energy difference with $P2_1/c$ in meV/f.u.	133.9	136.5

Table 3: The computed energy values for the $R3m$ of hafnia in the bulk and on SrTiO₃.

The $R3m$ -ES-SrTiO₃ phase is higher in energy than the $R3m$ -Bulk phase. This is to be expected as work is done to get the $R3m$ hafnia phase to deform. The simulations to compute the phonon dispersion relations were a little bit more difficult, as the unit cell for the $R3m$ -ES-SrTiO₃ phase comes close to the Brillouin zone phase transition point, with $|\vec{a}| = 6.683 \text{ \AA}$ and $|\vec{c}| = 10.04 \text{ \AA}$. The difference between the left and right hand side of equation 11 is only $0.0036 \text{ \AA}^{1/2}$. It is hard to say which Brillouin zone approximates the $R3m$ -ES-SrTiO₃ the best. That is why the phonon dispersion relations are shown of both the dispersion relations. All the dispersion relations of the $R3m$ -phases are shown in figure 31, 32 and 33.

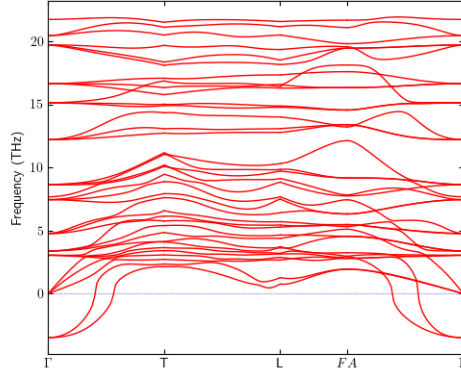


Figure 31: The computed phonon dispersion relation for the for the R3m-bulk phase of hafnia.

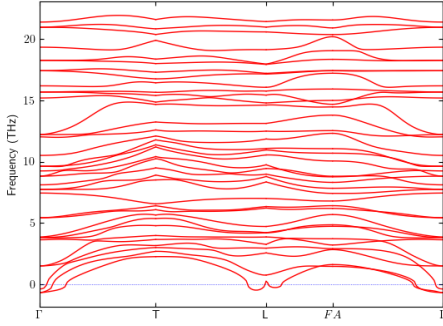


Figure 32: The computed phonon dispersion relation for the R3m-ES-SrTiO₃ of hafnia for $\sqrt{3}|\vec{a}| > \sqrt{2}|\vec{c}|$.

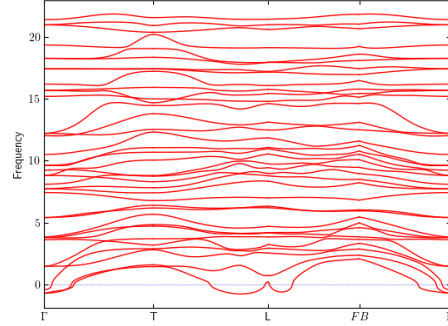


Figure 33: The computed phonon dispersion relation for the R3m-ES-SrTiO₃ of hafnia for $\sqrt{3}|\vec{a}| < \sqrt{2}|\vec{c}|$.

What first should be noted, it appears that there are no acoustic branches for the R3m-ES-SrTiO₃ phase for both Brillouin zones. This could mean that the result is unphysical. However, close to $f(\Gamma, 0 \text{ Hz})$ there are three small negative frequency dips, which all might be the acoustic branches. They might be displaced due to computational error, as also might be the case in the phonon dispersion relations of the Pbc_a and Pmn2₁ phases of hafnia. Furthermore both of the R3m-bulk and R3m-ES-SrTiO₃ phonon dispersion relations share a lot of similar optic branches at higher frequencies. Even though they are different 'phases', they do have a very similar lattice. Hence the results in figure 32 and 33 could be considered physical. As is shown in all phonon dispersion relations there are negative dips around the Γ point. The phonon dispersion relations of R3m-ES-SrTiO₃ also shows some minor dips at L . This dip is wider for the $\sqrt{3}|\vec{a}| < \sqrt{2}|\vec{c}|$ phonon dispersion

relation. It should be noted that the the negative dips are much stronger for the dispersion relation of R3m-Bulk. Again this hints to atom displacement and a phase change. It might be one of the phases described above in 4.1.2, or another phase that has not been discovered yet. However, that phase change would not be to the R3m-ES-SrTiO₃ phase, as it has a higher energy so the phase change would be to some other unknown phase. Furthermore the stronger negative dip denotes that the R3m-ES-SrTiO₃ phase is more stable then its bulk counterpart.

4.3 Properties of R3m phase hafnia grown on GaN

Using the methods described in subsection 3.4 one can find the energy versus \bar{c} lattice vector length relation for R3m-bulk, R3m-ES-SrTiO₃ and R3m-ES-GaN. After a couple runs for minimizing the energy values the relations are shown in figure 34, 35 and 36.

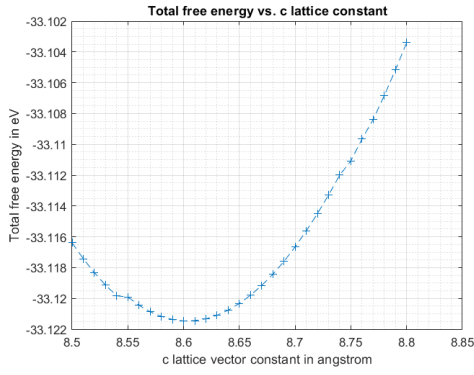


Figure 34: The computed energy versus the \bar{c} lattice vector length relation for R3m-bulk.

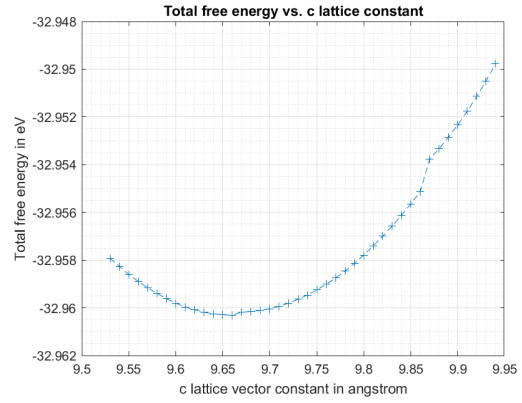


Figure 35: The computed energy versus the \bar{c} lattice vector length relation for R3m-ES-SrTiO₃.

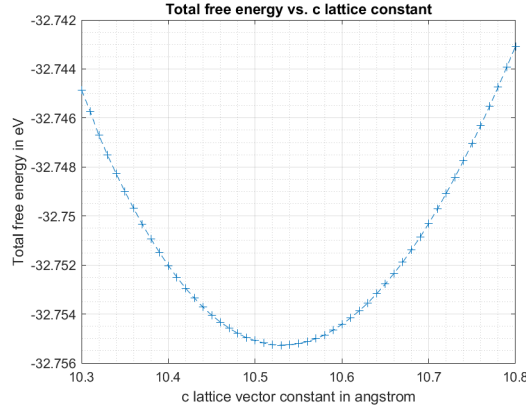


Figure 36: The computed energy versus the \bar{c} lattice vector length relation for R3m-ES-GaN.

All of the energy relations have a clear minimum and all the relations appear to be of parabolic form. What can be noticed is that in the relations for R3m-bulk and R3m-ES-SrTiO₃ there seems to be a discontinuity for R3m-bulk at 8.55 Å and for R3m-ES-SrTiO₃ at 9.66 Å and at 9.86 Å. For R3m-ES-SrTiO₃ the second discontinuity is more pronounced than the first one. The discontinuities could originate from computational error or from phase bound properties, but there are no hints to which one of these possibilities is more likely. The minimum values of the \vec{c} lattice vector compared to their literary counterparts by Wei et al. can be found in table 4 [8].

	R3m-bulk	R3m-ES-SrTiO ₃	R3m-ES-GaN
Computed $ \vec{c} $ by Wei et al. in Å [8]	8.741	10.041	-
Computed $ \vec{c} $ in Å	8.60	9.66	10.53

Table 4: The computed and literary values of $|\vec{c}|$ of the respective phases after minimalisation.

What table 4 makes clear is that there is some small deviation of the computed $|\vec{c}|$ with respect to their literary counterparts. For R3m-bulk the difference is about 0.14 Å and for R3m-ES-SrTiO₃ about 0.381 Å. Percentage wise this is a difference of respectively 1.6 % and 3.8 % for R3m-bulk and R3m-ES-SrTiO₃. These small deviations might be due to computational errors, but also due to the use of a different kind of software. The software used for the literary energy values is USPEX [38] [39] [40]. USPEX is a very different kind of software with respect to VASP. Just given the name of a phase and material, it tries to find a (meta)stable chemical composition of a phase. It does not need the unit cell geometry at all. USPEX uses a different approach than just energy minimalisation in the way VASP does in for example table 4. Furthermore, it uses different algorithms than VASP. Hence the deviations might be caused by the use of USPEX. Now for the energy values in figures 34, 35 and 36, in table 5 the minimum energies of the concerned figures are compared to the minimum energies in table 3. The difference between the two situations is that for the computations in table 3 data from Wei et al. is used for ionic relaxation with the \vec{a} and \vec{b} lattice vectors, together with the \vec{c} , being allowed to relax [8]. In the case of the computations depicted in figures 34, 35 and 36 the \vec{a} and \vec{b} vectors were not able to relax, while the \vec{c} via repeated calculations was allowed to relax.

	R3m-bulk	R3m-ES-SrTiO ₃	R3m-ES-GaN
Computed energy of the phases in eV/f.u. with flexible cell shape during relaxation as shown in table 3	-33.1113	-33.1087	-
Computed energy values of the phases in eV/f.u. with constrained \vec{a} and \vec{b} lattice vector during relaxation	-33.122	-32.960	-32.755

Table 5: The computed values of the energy of the respective phases after ionic relaxation with a flexible cell shape and after ionic relaxation with the \vec{a} and \vec{b} lattice vector constrained.

Earlier it was concluded that the energy calculations done for this research might be a rough approximation of the literary values, so the values found in table 5 might have a certain error margin. However, the results in table 5 might give a hint to the stability of the strained phases. This would give that strained R3m-bulk would be energetically favourable to the situation of a flexible cell shape during relaxation. The reverse would be true for R3m-ES-SrTiO₃. There is no

comparison material for R3m-ES-GaN as no data on the geometric structure of the R3m phase of hafnia was found in literature, so the found energy value only gives a rough estimate of the real energy value of R3m-ES-GaN. Assuming that the rough estimate comes close to the real energy value it shows that R3m-ES-GaN is less stable than both R3m-bulk and R3m-ES-SrTiO₃. Now for the found polarization values, they are shown in table 6.

	R3m-bulk	R3m-ES-SrTiO ₃	R3m-ES-GaN
Computed polarization values of the phases in $\mu C/cm^2$	5172	835	800

Table 6: The computed polarization values of the respective phases after ionic relaxation with the \vec{a} and \vec{b} lattice vector constrained.

What immediately becomes clear from the polarization values in table 6 is that the polarization values are unrealistically and unphysically large for all of the phases, especially for R3m-bulk. Hence one should not compare the polarization values of table 6 to the literary values as they are unphysical. It is not known what could be the source of this instability in the simulation, as the simulations work well up to a certain degree for calculating (physical) phonon dispersion relations and energy values. It could be one of the specific settings used, but pointing to which one is just guesswork, as trying to find the instable setting(s), if at all a certain option is the source of the instability, would take weeks as the computational load of the simulations using the methods used for the polarization calculation is very high. One possible source of instability might be that R3m in all calculations is (001) oriented instead of (111) oriented, which orientation was found in literature. As for the phonon dispersion relation of R3m-ES-GaN, a specific change in symmetry results takes place according to Phonopy after the ionic relaxation with the \vec{a} and \vec{b} lattice vector constrained. Due to the symmetry change a phase change occurred from R3m to Cm. Looking at the geometry of the unit cell after relaxation it seems that the cell shape of the unit cell is the same and the atomic positions have almost not changed so the phase change is unexpected. To give a complete overview of the possible correct phonon dispersion relation in figure 37 and 38 depict respectively a Cm phase approximation and a R3m phase approximation.

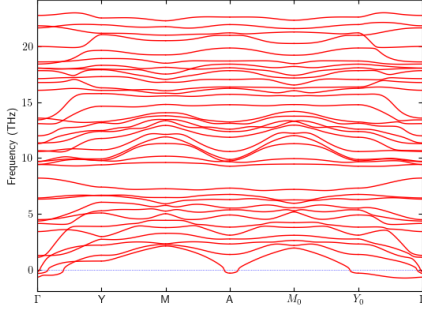


Figure 37: The computed phonon dispersion relation for the R3m-ES-GaN phase of hafnia in the Cm phase approximation.

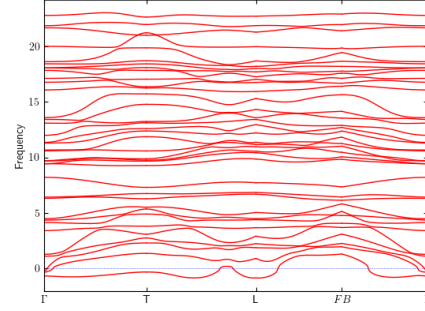


Figure 38: The computed phonon dispersion relation for the R3m-ES-GaN phase of hafnia in the R3m phase approximation.

Looking at the phonon dispersion relations in both upper figures both seem to be physically possible given there are acoustic branches present. The phonon dispersion relation in the Cm phase approximation in figure 37 seems to be more stable with respect to the R3m phase approximation counterpart in figure 38. Its negative frequency branch is only present in small parts of the domain whereas its counterparts negative frequency branch is negative on almost all of the domain. Furthermore it should be noted that the lower frequency branches of the Cm phase phonon dispersion relation look very similar to the ones in figure 32. Now for the interpolant of R3m-ES-SrTiO₃ and R3m-ES-GaN, R3m-ES-int, according to Phonopy the phase is R3 and not R3m. This is likely due to the fact that the geometry of R3m-int is computed by hand and due to small errors in atom positions a mirror plane is lost and so the R3m transitions to a R3 phase. The phonon dispersion relation for R3m-int is shown in figure 39.

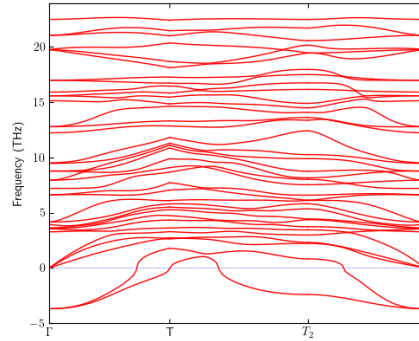


Figure 39: The computed phonon dispersion relation for the R3m-ES-int phase of hafnia, approximated by the R3 phase.

The phonon dispersion relation in figure 39 seems to be physical as there are clear acoustic branches. Over a large part of the domain negative frequency branches are present so the interpolant is likely not very physically stable. Even though R3m-ES-int is an interpolation of R3m-ES-SrTiO₃ and R3m-ES-GaN it is almost not visibly reflected in the phonon dispersion relation. If the phonon dispersion relation of figure 39 is compared to the ones in figure 32, 33, 37 and 38 there are almost no points of similarity. The most visible one is frequency band around 13 – 15 THz follows a similar pattern with the other phonon bandplots. The fact that R3m-ES-int shows almost no similarities might hint that the result is not correct but this is not for sure.

5 Conclusion

In this thesis, we have researched the various phases of hafnia. Using data from The Materials project [10] [32], research done by Wei et al. [8] and Huan et al. [9] we were able to research the $P2_1/c$, $Fm-3m$, $Pbca$, $P4_2/nmc$, $Pmn2_1$, $Pca2_1$, $P4_2/mnm$, $Pnma$ and $R3m$ phases of hafnia. Making use of the Bilbao Crystallographic Server in combination with the retrieved data the geometry of unit cells and the atom position within the unit cell for the hafnia phases could be constructed [33] [34]. Using Density Functional Theory, DFT for short, in combination with the software package Vienna Ab initio Simulation Package, VASP for short, various properties of the hafnia phases could be computed [23] [24] [25] [26] [27]. As input to VASP the unit cell geometry is used, represented in the file POSCAR [28], in combination with a set of options in the INCAR and KPOINTS file [29] [30] and a set of pseudopotentials in the POTCAR file. These files are explained in section 3.1.

Using the ionic relaxation mode in VASP we computed the energy values of the researched phases (see section 3.2). The results are shown in table 1. The found energy values were compared to data from Wei et al. and Clima et al., as is shown in table 2 [8] [5]. The maximum difference between the computed and literary values is $24 \text{ meV}/f.u.$ less than an order of magnitude with respect to the literary values. It could be concluded that the computation of the energy values with our method gives a rough estimation of the literary values.

Using the second derivatives/Hessian matrix mode of VASP, we computed the phonon dispersion relations of the researched phases (see section 3.3). The phonon dispersion relations are shown from figure 17 to figure 33. All the phonon dispersion relations display physical situations as they all have acoustic branches. When compared to material by Huan et al., except for the $Fm-3m$ phase, all of the comparable phonon dispersion relations are similar to their literary counterparts, also shown between figure 17 to 33 [9]. The $P4_2/nmc$ phase shows small negative frequency dips around the Γ point, which points to instability of the phase. This likely due the fact that the $p4_2/nmc$ phase is the parent phase of two ferroelectric orthorhombic phases. The conclusion is that our simulations in VASP create validable phonon dispersion relations.

Using both the ionic relaxation and second derivatives/Hessian matrix mode in VASP energy values, phonon dispersion relations and polarization values of interested $R3m$ phases grown on $SrTiO_3$ and GaN could be computed (see section 3.4). To do so the \vec{a} and \vec{b} lattice vector are constrained. The ionic relaxation processes of bulk $R3m$ phase and it strained on $SrTiO_3$ and GaN can be seen in figure 34 to 36. The ionic relaxation processes show well defined minima. The difference of the length of the \vec{c} lattice vector with the computed unstrained counterparts the \vec{a} and \vec{b} lattice vector counterparts is at most 3.8 %. The energy values corresponding to the minima hint that $R3m$ strained on GaN is energetically less favourable than $SrTiO_3$ (see table 5). The polarization values retrieved from the computations show unrealistic high values and should be used for comparisons. The source of the instability in the simulation is unknown. The phonon dispersion relations of the $R3m$ phase of hafnia grown on GaN shows to be a Cm phase instead of $R3m$, see figure 37. A phonon dispersion relation of an interpolant between the $R3m$ phase grown on $SrTiO_3$ and GaN can be found in figure 39, it shows now particular point(s) of interest.

Summarizing the answers to the research questions, we were able to reproduce phonon spectra up to a comparable level and the computed energy levels give a rough estimation. From the $R3m$ phase of hafnia we were able to produce phonon dispersion relation and energy value data on both $SrTiO_3$ and GaN , but no polarization data as the data is unphysical for an unknown reason. A relation between the \vec{c} lattice vector and the energy of the unit cell has been found for both the $SrTiO_3$ and GaN substrate.

6 Discussion

During the bachelor theses some points of consideration came to light. Some are denoted below to bring up a discussion about and a starting point for possible research in the future.

During the research the computation of the results for figure 34 to 36 was done using several methods and it took some time to find the right method to compute them. In the end it was chosen to do it with the help of the jobscript in appendix A, but another method might be interesting for future research. Before working with the jobscript the software Gadget was used [41]. Due to ICT problems we did not get it to work but Gadget might make computations easier for future research as it gives more options and flexibility when using it together with VASP, instead of using VASP alone. For example it would have been possible to simulate the \vec{a} and \vec{b} lattice vector being constrained without creating a specific jobscript, which was needed because VASP was not able to constrain one or more lattice vectors specifically. Using Gadget in future research might give various new insights on hafnia.

The research done using VASP in this bachelor theses is very simplified, it uses the (001) orientation of phases instead of (111) orientation, and only pure hafnia is considered. This might have oversimplified the problem and might have been the source the unphysical polarization values. For future research I would recommend to first change the (001) orientation of the R3m phase of hafnia to the (111) orientation and then redo the computations done in this bachelor thesis of the polarization values of bulk and constrained R3m phase of hafnia.

Several times in this bachelor thesis a possible reason for deviations of computed data when compared to their literary counterparts is the possible or certain difference in settings used for simulations. Redoing the research with all the specific settings of computations in literature would take too much time for a bachelor thesis, so that has not happened yet. For future research this might be a starting point to find data on the R3m phase confirming literary data. The same goes for the use of other software for ionic simulations than just VASP. In the literature about the R3m phase of hafnia besides VASP the ABINIT software package was also used for example.

For this bachelor thesis the geometric structure data of the phases of hafnia was retrieved mainly from the Materials project [10] [32], but also from research by Wei et al. [8] and Huan et al. Wei et al. and several researchers have used USPEX for retrieving geometric structure data of thin films they have created in reality. The USPEX software package might make it easier to find fitting structure data for future research. Just using a name of a phase and material will give, after a computation, geometric structure data. Furthermore the data by USPEX on the phases of hafnia that has been used in research is very well comparable to literary data (see the paper by Wei et al. for further details [8]).

To not make the size of this bachelor thesis not too large research on the R3 phase of hafnia has not been performed. The sample of R3m phase of hafnia grown on GaN on the University of Twente was found to have more resemblance with the R3 phase than the R3m phase [42]. For future research it might be of interest to do calculations on the R3 phase of hafnia.

Bibliography

- [1] “A century of ferroelectricity”. In: *Nature Materials* 19.2 (Feb. 2020), pp. 129–129. ISSN: 1476-4660. DOI: 10.1038/s41563-020-0611-1.
- [2] A. Bhalla A. S. Saxena. *Ferroelectricity: 100 years on*. Nov. 2020. URL: <https://physicsworld.com/a/ferroelectricity-100-years-on>.
- [3] J. F. Scott. “Applications of Modern Ferroelectrics”. In: *Science* 315.5814 (2007), pp. 954–959. ISSN: 0036-8075. DOI: 10.1126/science.1129564.
- [4] Shashank Priya et al. “A Review on Piezoelectric Energy Harvesting: Materials, Methods, and Circuits”. In: *Energy Harvesting and Systems* 4.1 (2017), pp. 3–39. DOI: 10.1515/ehs-2016-0028.
- [5] S. Clima et al. “Identification of the ferroelectric switching process and dopant-dependent switching properties in orthorhombic HfO₂: A first principles insight”. In: *Applied Physics Letters* 104.9 (2014), p. 092906. DOI: 10.1063/1.4867975.
- [6] M.L.C.M. Henckens, P.P.J. Driessen, and E. Worrell. “Metal scarcity and sustainability, analyzing the necessity to reduce the extraction of scarce metals”. In: *Resources, Conservation and Recycling* 93 (2014), pp. 1–8. ISSN: 0921-3449. DOI: 10.1016/j.resconrec.2014.09.012.
- [7] Patrick Wäger. “Scarce metals - Applications, supply risks and need for action”. In: *Notizie di Politeia* 27 (Jan. 2011), pp. 57–66.
- [8] Yingfen Wei et al. “A rhombohedral ferroelectric phase in epitaxially-strained Hf_{0.5}Zr_{0.5}O₂ thin films”. In: *Nature Materials* 17 (Dec. 2018). DOI: 10.1038/s41563-018-0196-0.
- [9] Tran Doan Huan et al. “Pathways towards ferroelectricity in hafnia”. In: *Phys. Rev. B* 90 (6 Aug. 2014), p. 064111. DOI: 10.1103/PhysRevB.90.064111.
- [10] Anubhav Jain et al. “The Materials Project: A materials genome approach to accelerating materials innovation”. In: *APL Materials* 1.1 (2013), p. 011002. ISSN: 2166532X. DOI: 10.1063/1.4812323.
- [11] V. M. Fridkin and S. Ducharme. *General features of the intrinsic ferroelectric coercive field*. 2001. URL: <https://link.springer.com/article/10.1134/1.1386472>.
- [12] D. P. Burke and W. M. Rainforth. “Intermediate rhombohedral (r-ZrO₂) phase formation at the surface of sintered Y-TZP’s”. In: *Journal of Materials Science Letters* 16.11 (June 1997), pp. 883–885. ISSN: 1573-4811. DOI: 10.1023/A:1018571601638.
- [13] G.A. Kalinovskaya, F.M. Spiridonov, and L.N. Komissarova. “Phase equilibria in the HfO₂-Sc₂O₃ system”. In: *Journal of the Less Common Metals* 17.2 (1969), pp. 151–159. ISSN: 0022-5088. DOI: 10.1016/0022-5088(69)90048-4.
- [14] Hideo Hasegawa. “Rhombohedral phase produced in abraded surfaces of partially stabilized zirconia (PSZ)”. In: *Journal of Materials Science Letters* 2.3 (1983), pp. 91–93. DOI: 10.1007/bf00722220.
- [15] H. Hasegawa, T. Hioki, and O. Kamigaito. “Cubic-to-rhombohedral phase transformation in zirconia by ion implantation”. In: *Journal of Materials Science Letters* 4.9 (1985), pp. 1092–1094. DOI: 10.1007/bf00720424.

- [16] Yuke Zhang et al. “Effects of Strain and Film Thickness on the Stability of the Rhombohedral Phase of HfO_2 ”. In: *Phys. Rev. Applied* 14 (1 July 2020), p. 014068. DOI: 10.1103/PhysRevApplied.14.014068.
- [17] S Perkowitz. *Phonon*. Jan. 2018. URL: <https://www.britannica.com/science/phonon>.
- [18] J. R. Hook and H. E. Hall. *Solid state physics*. Wiley, 2013.
- [19] K. Parlinski. “Lattice Dynamics: Vibrational Modes”. In: *Encyclopedia of Condensed Matter Physics*. Ed. by Franco Bassani, Gerald L. Liedl, and Peter Wyder. Oxford: Elsevier, 2005, pp. 98–102. ISBN: 978-0-12-369401-0. DOI: 10.1016/B0-12-369401-9/00509-X.
- [20] Astrid Marthinsen. *Fundamentals and applications of Density Functional Theory*. Feb. 2016. URL: <https://www.youtube.com/watch?v=SXvhDLCycxc>.
- [21] Martijn Marsman. *VASP Workshop at NERSC: Basics: DFT, plane waves, PAW method, electronic minimization, Part 1*. Dec. 2016. URL: <https://www.youtube.com/watch?v=vJkNv095Aj8>.
- [22] Martijn Marsman. *VASP basics: DFT, PW and PAW*. URL: https://www.vasp.at/wiki/images/5/5d/VASP_lecture_Basics.pdf.
- [23] G. Kresse and J. Hafner. “Ab initio molecular dynamics for liquid metals”. In: *Phys. Rev. B* 47 (1 Jan. 1993), pp. 558–561. DOI: 10.1103/PhysRevB.47.558.
- [24] G. Kresse and J. Furthmüller. “Efficiency of ab-initio total energy calculations for metals and semiconductors using a plane-wave basis set”. In: *Computational Materials Science* 6.1 (1996), pp. 15–50. ISSN: 0927-0256. DOI: 10.1016/0927-0256(96)00008-0.
- [25] G. Kresse and J. Furthmüller. “Efficient iterative schemes for ab initio total-energy calculations using a plane-wave basis set”. In: *Phys. Rev. B* 54 (16 Oct. 1996), pp. 11169–11186. DOI: 10.1103/PhysRevB.54.11169.
- [26] G Kresse and J Hafner. “Norm-conserving and ultrasoft pseudopotentials for first-row and transition elements”. In: *Journal of Physics: Condensed Matter* 6.40 (Oct. 1994), pp. 8245–8257. DOI: 10.1088/0953-8984/6/40/015.
- [27] G. Kresse and D. Joubert. “From ultrasoft pseudopotentials to the projector augmented-wave method”. In: *Phys. Rev. B* 59 (3 Jan. 1999), pp. 1758–1775. DOI: 10.1103/PhysRevB.59.1758.
- [28] VASP software GmbH. *POSCAR*. URL: <https://www.vasp.at/wiki/index.php/POSCAR>.
- [29] VASP software GmbH. *INCAR*. URL: <https://www.vasp.at/wiki/index.php/INCAR>.
- [30] VASP software GmbH. *KPOINTS*. URL: <https://www.vasp.at/wiki/index.php/KPOINTS>.
- [31] VASP software GmbH. *POTCAR*. URL: <https://www.vasp.at/wiki/index.php/POTCAR>.
- [32] Shyue Ping Ong et al. “Python Materials Genomics (pymatgen): A robust, open-source python library for materials analysis”. In: *Computational Materials Science* 68 (Feb. 2013), pp. 314–319. ISSN: 09270256. DOI: 10.1016/j.commatsci.2012.10.028.
- [33] Mois I. Aroyo et al. “Bilbao Crystallographic Server. II. Representations of crystallographic point groups and space groups”. In: *Acta Crystallographica Section A* 62.2 (Mar. 2006), pp. 115–128. DOI: 10.1107/S0108767305040286.
- [34] Mois Aroyo et al. “Bilbao Crystallographic Server: I. Databases and crystallographic computing programs”. In: *ZEITSCHRIFT FÜR KRISTALLOGRAPHIE* 221 (Jan. 2006), pp. 15–27. DOI: 10.1524/zkri.2006.221.1.15.

- [35] VASP software GmbH. *IBRION*. URL: <https://www.vasp.at/wiki/index.php/IBRION>.
- [36] VASP software GmbH. *EDIFFG*. URL: <https://www.vasp.at/wiki/index.php/EDIFFG>.
- [37] A Togo and I Tanaka. “First principles phonon calculations in materials science”. In: *Scr. Mater.* 108 (Nov. 2015), pp. 1–5.
- [38] Andriy O. Lyakhov et al. “New developments in evolutionary structure prediction algorithm USPEX”. In: *Computer Physics Communications* 184.4 (2013), pp. 1172–1182. ISSN: 0010-4655. DOI: 10.1016/j.cpc.2012.12.009.
- [39] Artem R. Oganov and Colin W. Glass. “Crystal structure prediction using ab initio evolutionary techniques: Principles and applications”. In: *The Journal of Chemical Physics* 124.24 (2006), p. 244704. DOI: 10.1063/1.2210932.
- [40] Colin Glass, Artem Oganov, and Nikolaus Hansen. “USPEX—Evolutionary crystal structure prediction”. In: *Computer Physics Communications* 175 (Dec. 2006), pp. 713–720. DOI: 10.1016/j.cpc.2006.07.020.
- [41] Tomáš Bučko, Jürgen Hafner, and János G. Ángyán. “Geometry optimization of periodic systems using internal coordinates”. In: *The Journal of Chemical Physics* 122.12 (2005), p. 124508. DOI: 10.1063/1.1864932.
- [42] Laura Bégon-Lours et al. “Stabilization of phase-pure rhombohedral HfZrO₄ in pulsed laser deposited thin films”. In: *Phys. Rev. Materials* 4 (4 Apr. 2020), p. 043401. DOI: 10.1103/PhysRevMaterials.4.043401.

A The jobscript of the ionic relaxation of the R3m phase of hafnia constrained on SrTiO₃ and GaN

The first part of the altered jobscript used in section 4.3 can be found in figure 40. The second part can be found in figure 41. Note that a piece of code is cut off in the code in the middle, as it is not of interest for any explanation.

```
#!/bin/bash
#SBATCH -t 48:00:00
#SBATCH -p cms13
#SBATCH -N 2 --tasks-per-node=8
#SBATCH -J R3mv2
#SBATCH --output=R3m.out
#SBATCH --error=R3m.err
#SBATCH --mail-type=all
#SBATCH --exclusive
#SBATCH --mail-user=[REDACTED]utwente.nl
ulimit -s unlimited
module load mpi/intel/4.1.0.024
module load mpi/openmpi/1.7.4
module load mkl/11.0.1
module load fftw/3.3.3
module load compiler/intel/13.1.117
cd $PWD
rm WAVECAR SUMMARY.fcc
for i in 10.30 10.31 10.32 10.33 10.34 10.35 10.36 10.37 10.38 10.39 10.40
do
cat > POSCAR <<!
New Structure
1.0
  6.4320000000      0.0000000000      0.0000000000
 -3.2160000000     5.5702753971      0.0000000000
  0.0000000000     0.0000000000      $i
Hf 0
12 24
Direct
  0.496107000      0.503893000      0.603983000
  0.162773000      0.837227000      0.937317000
  0.829440000      0.170560000      0.270650000
  0.829440000      0.658880000      0.270650000
  0.341120000      0.170560000      0.270650000
  0.496107000      0.992213000      0.603983000
  0.674453000      0.837227000      0.937317000
  0.162773000      0.325547000      0.937317000
  0.007787000      0.503893000      0.603983000
  0.666667000      0.333333000      0.886113000
  0.333333000      0.666667000      0.219447000
```

Figure 40: The first part of the altered jobscript used in section 4.3.


```

0.333333000      0.666667000      0.016147000
0.000000000      0.000000000      0.349480000
!
echo "a= $i" ; srun ██████████ vasp/vasp5.3
V=`grep volume/ion OUTCAR|awk '{print$5}'`
E=`awk '/F=/ {print $0}' OSZICAR`
P=`grep "Ionic dipole moment" OUTCAR | awk '{print$0}'`
echo $i $V $E $P >>SUMMARY.dat
echo $V $E $P >>SUMMARYVOL.dat
cat CONTCAR >> contcars
cat OSZICAR >> oszicars
cat OUTCAR >> outcars
done
cat SUMMARY.fcc
cat SUMMARYVOL.dat

```

Figure 41: The second part of the altered jobscript used in section 4.3.

The first seventeen rules of the altered jobscript are the same as the jobscript in figure 11. After that the job script is changed. The 18th line removes the WAVECAR and SUMMARY.fcc files, as WAVECAR is not needed for the simulations and SUMMARY.fcc is created during the run of the jobscript. Then from line 19th on to the third last line the jobscript contains a for-loop. The for-loop goes through three steps every time SLURM runs through it. Firstly, it changes the POSCAR present in the execution folder to change the \vec{c} lattice vector length. Secondly, given the changed POSCAR it runs VASP. Finally, it stores information needed for calculations of the energy minimisation and polarization calculations in SUMMARY.dat and SUMMARYVOL.dat and it stores all of the CONTCARS, OSZICARS and OUTCARS created during the jobscript run. The first step is described in the jobscript from the 21th line to the fourteenth last line. The second step is performed on the twelveth last line and the third step is performed from the eleventh last to the fourth last line. The \vec{c} lattice vector (length) is represented by the variable \$i, which is changed every time SLURM runs through the jobscript. The 19th line gives the \vec{c} lattice vector lengths to be researched and can be set by the user of the jobscript. The last two lines print the summary files of the jobscript run to which the needed information for computations are saved.